photonics

MDPI

Article

Enhanced Upconversion Photoluminescence of $LiYF_4$: Yb^{3+}/Ho^{3+} Crystals by Introducing Mg^{2+} Ions for Anti-Counterfeiting Recognition

Dongdong Li [1,*,†], Jinghua Wang [1,†], Chong Wang [1] and Jiangbo She [2]

1 School of Electronic Engineering, Xi'an University of Posts & Telecommunications, Xi'an 710121, China
2 State Key Laboratory of Transient Optics and Photonics, Xi'an Institute of Optics and Precision Mechanics, Chinese Academy of Sciences, Xi'an 710119, China
* Correspondence: dongdong19821111@163.com; Tel.: +86-153-5364-5227
† These authors contributed equally to this work.

Abstract: By doping appropriate lanthanide ions, $LiYF_4$ as a host luminescent material can simultaneously exhibit bright visible-light emission. A series of $LiYF_4$:Yb^{3+}/Ho^{3+} microparticles with different Mg^{2+} doping concentrations were synthesized and investigated. The crystal structure of the synthesized microparticles was tested by X-ray diffraction (XRD). Notably, a significant increase in the upconversion photoluminescence intensity of upconversion microparticles (UCMPs) was obtained by introducing Mg2+ ions under 980 nm laser excitation, and achieved a maximum level when the concentration of Mg^{2+} ions was 8 mol%. Additionally, the practicality of the resultant UCMPs used as the raw material of anti-counterfeiting ink was systematically investigated. These results prove that the Mg^{2+}-doped $LiYF_4$:Yb^{3+}/Ho^{3+} are very promising as screen-printing materials for anti-counterfeiting recognition labels.

Keywords: hydrothermal synthesis; $LiYF_4$:Yb^{3+}/Ho^{3+}; anti-counterfeiting identification; screen printing

Citation: Li, D.; Wang, J.; Wang, C.; She, J. Enhanced Upconversion Photoluminescence of $LiYF_4$: Yb^{3+}/Ho^{3+} Crystals by Introducing Mg^{2+} Ions for Anti-Counterfeiting Recognition. *Photonics* **2022**, *9*, 614. https://doi.org/10.3390/photonics9090614

Received: 23 July 2022
Accepted: 24 August 2022
Published: 30 August 2022

1. Introduction

Compared with other luminescent materials (e.g., organic dye, quantum dots, etc.), rare-earth-doped luminescent materials have many advantages, such as sharp emission and long lifetime, good photochemical and thermal stability, etc. [1]. The luminescent properties of lanthanide-doped fluoride materials are mainly subject to the host matrix, sensitizers, and activators [2–5]. Hence, optimal host–dopant combinations are necessary for an efficient UC luminescence process. It is universally known that the UC efficiency of rare-earth ions depends largely on the phonon energy of the matrix. $LiYF_4$ is also considered to be an ideal alternative method, which is likely to inhibit non-radiative relaxation due to its low phonon energy [6]. In addition, the $LiYF_4$ host can simultaneously exhibit bright visible-light emission by doping with appropriate lanthanides. Herein, $LiYF_4$ was selected as the host material, and the combination Yb^{3+}/Ho^{3+} was used as a sensitizer/activator to increase the excitation of the photons.

The doping of non-rare-earth ions is regarded as a promising approach for the improvement of UC [6–10]. Zhou et al. reported the enhancement of green upconversion luminescence in tetrahedral $LiYF_4$:Yb/Er nanoparticles by doping with Mn^{2+} ions [6]. Li et al. synthesized $NaLnF_4$ UCNPs via a simple M^{2+} (Mg^{2+}, Co^{2+}) doping method [7]. Yang et al. synthesized Mg^{2+}-doped hexagonal-phase $NaGdF_4$:Yb^{3+}, Er^{3+} nanocrystals; the results show that the intensity of UC emission increased significantly as a result of Mg^{2+} doping [8]. The results show that overall UCL is enormously enhanced after doping with Mg^{2+} (≈27.5-fold). Ding et al. synthesized Li^{+}-doped β-$NaGdF_4$:Ln^{3+} nanocrystals, and a significant enhancement of UC emission in the β-$NaGdF_4$:Ln^{3+} nanocrystals was observed [9]. Ding et al. synthesized a Mn^{+}-doped core–shell–shell nanoarchitecture, and the NIR-to-red upconversion emission was efficiently promoted [10]. Dopant-enhanced upconversion nanoparticles (UCNPs) have attracted great interest for anti-counterfeiting for their specific UC luminescence property of emitting higher-efficiency shorter wavelengths via near-infrared (NIR) excitation [11–15].

In this work, a series of $LiYF_4:Yb^{3+}/Ho^{3+}$ UCMPs with different Mg^{2+} doping concentrations were successfully prepared via hydrothermal synthesis methods. In $LiYF_4$ crystals, because the radius of Mg^{2+} (0.72 Å) ions is less than that of Y^{3+} (0.90 Å), the incorporation of Mg^{2+} ions replaces some of the Y^{3+} ions or fills the crystal gap, resulting in the shrinkage and expansion of the main lattice and the asymmetry of local crystal field. The symmetry of the $LiYF_4$ local crystal field is changed by the doping with Mg^{2+} ions, so as to affect the UC luminescence efficiency of the product [16,17]. The crystal structure and photoluminescence intensity of $LiYF_4:Yb^{3+}/Ho^{3+}$ UCMPs were characterized. Finally, the fluorescence imaging experiment was carried out. The imaging results prove that the prepared UCMPs can be applied to screen printing.

2. Experimental Section

Mg^{2+}-ion-doped $LiYF_4:Yb^{3+}/Ho^{3+}$ micron crystals were prepared via hydrothermal synthesis. The specific preparation process was as follows: First, 1 mmol ethylenediaminetetraacetic acid (EDTA) powder was dissolved in 20 mL of deionized water in a beaker and stirred continuously under the auxiliary condition of constant-temperature heating at 60 °C to form solution A. Secondly, 1 mmol rare-earth nitrate was dissolved in 10 mL of deionized water and subjected to ultrasonic treatment for 10 min to form a mixed solution B. The rare-earth nitrate included $Y(NO_3)_3{\cdot}6H_2O$, $Mg(NO_3)_2{\cdot}6H_2O$, $Yb(NO_3)_3{\cdot}5H_2O$, and $Ho(NO_3)_3{\cdot}5H_2O$, with the proportions of 0.79-x, x, 0.2, and 0.01, respectively. X is the doping amount of Mg^{2+}. Solution A and solution B were mixed and stirred well. A mixed solution of 20 mmol LiF and 5 mmol NH_4F was dissolved in water to form solution C (5 mL). Finally, solution C was dropped slowly into the mixed solution and continuously stirred for about 30 min to form a milky white liquid. Finally, the mixture was put into the autoclave, and maintained for 48 h at 230 °C. The products were washed with a mixture of deionized water and ethanol (volume, 1:1) and centrifuged several times. Then, they were dried in a vacuum-drying oven at 60 °C for 12 h and, finally, the samples were ground and collected.

The X-ray diffraction (XRD) patterns of the products demonstrated their crystal structure and phase identification, and were recorded using a BRUKER D8 ADVANCE type X-ray diffractometer with Cu Kα radiation (λ is 0.1546 nm). The elemental content of the sample was measured using an inductively coupled plasma optical emission spectrometer (ICP-OES, Agilent 5110), see Table S1. A power-adjustable 980 nm laser diode (0 to 2W) was selected as a pump light source. The photoluminescence spectra were obtained using a Hitachi F-4500 fluorescence spectrophotometer (1.0 nm for spectral resolution (FWHM) of the spectrophotometer and 400 V for PMT voltage) at room temperature. The camera employed for taking photographs in the imaging experiments was a high-performance CCD camera produced by Andorra, UK.

3. Results and Discussion

The XRD results of $LiYF_4:Yb^{3+}/Ho^{3+}$ UCMPs with different Mg^{2+} doping concentrations are shown in Figure 1. The concentrations of $LiYF_4:Yb^{3+}/Ho^{3+}$ UCMPs with Mg^{2+} ion doping were 0 mol%, 4 mol%, 6 mol%, 8 mol%, 10 mol%, and 12 mol%. The main diffraction peaks were 100, 110, 101, 200, 111, 201, 210, 002, 300, 211, 102, 112, 220, 311, 312, and 302. The diffraction peaks of the $LiYF_4:Yb^{3+}/Ho^{3+}$ UCMPs generally coincided with the PDF standard card (PDF: 17-0874).There were no other miscellaneous peaks, even with high-concentration Mg^{2+} ion doping, indicating that pure UCMPs were prepared.

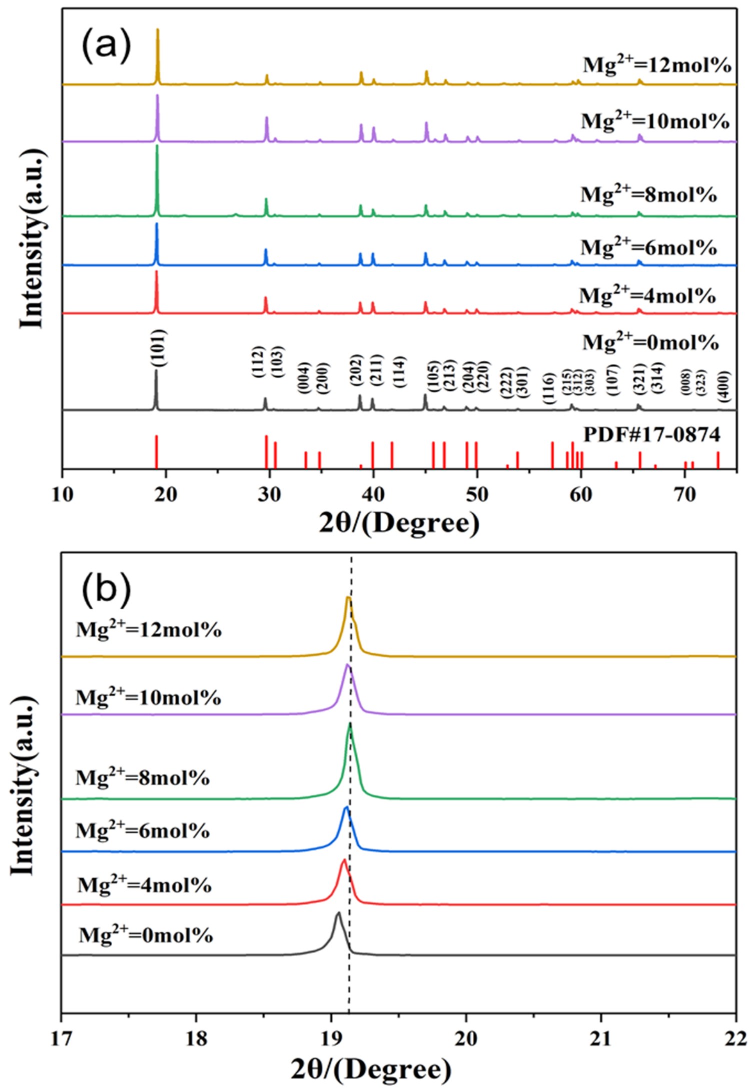

Figure 1. (**a**) XRD diffraction pattern of Mg^{2+}-doped $LiYF_4$:Yb^{3+}/Ho^{3+} UCMPs; (**b**) diffraction peak of Mg^{2+}-doped $LiYF_4$:Yb^{3+}/Ho^{3+} UCMPs around 19°.

As a result, Figure 1a shows the XRD pattern of Mg^{2+}-doped $LiYF_4$:Yb^{3+}/Ho^{3+} around 19°. As seen from the local magnification of the XRD images, the diffraction peak shifts to the right with the increase in Mg^{2+} concentration. The angular movement of the main diffraction peak reaches the limit when the Mg^{2+} doping concentration is 8 mol%. When the concentration of Mg^{2+} ions exceeds 8 mol%, the diffraction peak of the nanocrystal starts to move to the left again.

In $LiYF_4$ crystal, because the radius of Mg^{2+} (0.72 Å) ions is less than that of Y^{3+} (0.90 Å), the incorporation of Mg^{2+} ions replaces some of the Y^{3+} ions or fills the crystal gap, resulting in the shrinkage and expansion of the main lattice and the asymmetry of the local crystal field. When the doping concentration of Mg^{2+} ions is 0–8 mol%, the crystal shrinks, and the main diffraction peak of XRD moves to the right. When the doping concentration of Mg^{2+} ions is greater than 8 mol%, the lattice structure expands, and the main diffraction peak begins to move to the left. The symmetry of the $LiYF_4$ local crystal field is changed by the doping of Mg^{2+} ions, so as to affect the UC luminescence efficiency of the product [16,17].

$$2d\sin\theta = n\lambda \quad (1)$$

In the Bragg's law formula, λ, d, and θ are the diffraction wavelength, the distance between planes, and the diffraction angle, respectively. According to Formula (1), when a certain amount of Mg^{2+} ions are added, some Mg^{2+} ions will enter the lattice gap of $LiYF_4$, increasing the distance d between planes and reducing the diffraction angle θ. As the concentration of Mg^{2+} ions decreases, the $LiYF_4:Yb^{3+}/Ho^{3+}$ lattice expands, so the XRD moves to a low angle.

As shown in Figure 2, the $LiYF_4:Yb^{3+}/Ho^{3+}$ UCMPs with different Mg^{2+} impurity concentrations were tested by SEM. In Figure 2, the samples have good crystallinity, and the morphology of the samples is similar to a biconical octahedron structure. The morphology is regular and the dispersion is mainly uniform. The average size of the microcrystals is about 55 μm in length and 30 μm in width under different Mg^{2+} ion doping concentrations.

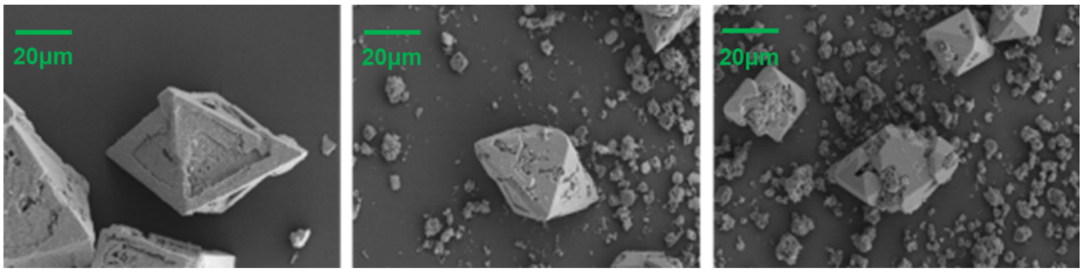

(**a**) (**b**) (**c**)

Figure 2. SEM of Mg^{2+}-doped $LiYF_4:Yb^{3+}/Ho^{3+}$ UCMPs. (**a**) Mg^{2+}=0 mol%, (**b**) Mg^{2+}=8 mol%, (**c**) Mg^{2+}=12 mol%.

The photoluminescence was investigated as a function of the change in Mg^{2+} doping concentration. The $LiYF_4:Yb^{3+}/Ho^{3+}$ UCMPs with Mg^{2+} doping concentrations of 0%, 4%, 6%, 8%, 10%, and 12% were selected for fluorescence spectroscopy tests.

Figure 3 shows the photoluminescence spectra of different Mg^{2+} doping concentrations of $LiYF_4:Yb^{3+}/Ho^{3+}$UCMPs under 980 nm laser excitation. As shown in Figure 3, the photoluminescence intensity increased continuously as the Mg^{2+} doping concentration changed from 0 mol% to 8 mol%. The photoluminescence intensity reached the maximum as the Mg^{2+} doping concentration reached 8 mol%. However, when the Mg^{2+} doping concentration was greater than 8 mol%, the photoluminescence intensity gradually weakened with the increase in Mg^{2+} doping concentration. Compared with the samples without Mg^{2+} doping, the UC luminescence intensity of $LiYF_4:Yb^{3+}/Ho^{3+}$ UCMPs with a doping concentration of 8 mol% was increased by about fourfold. It was thus proven that the adding Mg^{2+} ions into $LiYF_4:Yb^{3+}/Ho^{3+}$ micron crystals can enhance the upconversion luminescence intensity effectively. Because the incorporation of Mg^{2+} ions changes the symmetry of the crystal field, the crystal field distortion also affects the UC luminescence efficiency of Ho^{3+} ions, improving the UC luminescence performance of the $LiYF_4:Yb^{3+}/Ho^{3+}$ crystals [7,8].

The energy level transition diagram of Mg^{2+}-doped $LiYF_4:Yb^{3+}/Ho^{3+}$ under the irradiation of 980 nm lasers is shown in Figure 4. After the Yb^{3+} ions absorb laser energy, they first transition from the $^2F_{7/2}$ energy level to the $^2F_{5/2}$ energy level, followed by cross-relaxation and energy transfer with Ho^{3+}ions. Then, a series of radiative transitions of Ho^{3+} ions are formed through the energy transfer (ET_1) process, and through energy transfer (ET_2, ET_3) caused by cross-relaxation processes (CR_1 and CR_2) between two close Yb^{3+} and Ho^{3+} ions [18]. This results in the green UC emission of Ho^{3+} ions at 535 nm ($^5F_4 \rightarrow {}^5I_8$) and 543 nm ($^5S_2 \rightarrow {}^5I_8$), the red UC emission of Ho^{3+} at 638 nm ($^3K_8$, $^5F_2$, $^5F_3 \rightarrow {}^5I_7$) and 657 nm ($^5F_5 \rightarrow {}^5I_8$), and near-infrared UC emission of Ho^{3+} ions at 750 nm ($^5F_4$, $^5S_2 \rightarrow {}^5I_7$).

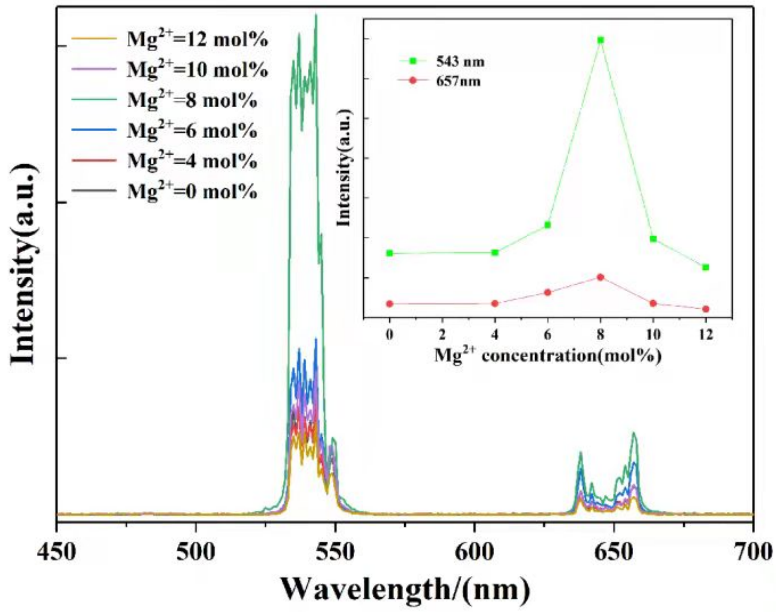

Figure 3. Photoluminescence spectra of $LiYF_4:Yb^{3+}/Ho^{3+}$ UCMPs with different Mg^{2+} doping concentrations.

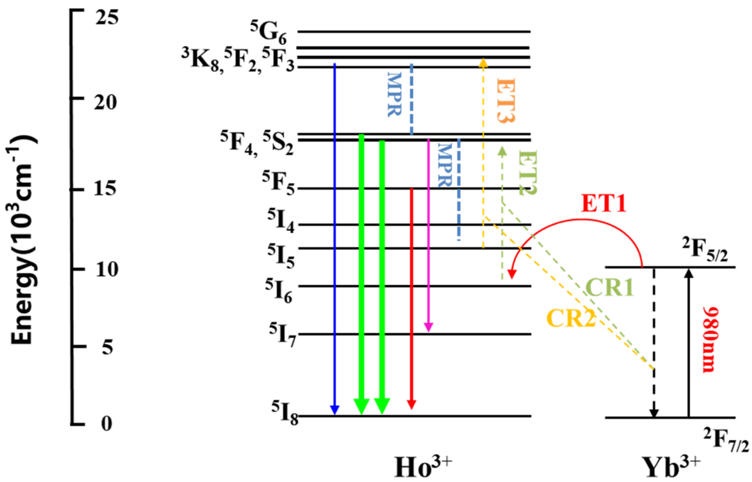

Figure 4. Schematic diagram of energy level transition of Mg^{2+}−doped $LiYF_4:Yb^{3+}/Ho^{3+}$ UCMPs.

The red–green light intensity ratio is an essential standard to evaluate the luminescence performance of luminescent materials. Figure 5a shows the changes in the upconversion red–green light intensity ratio ($R/G = I_{657nm}/I_{543nm}$) of $LiYF_4:Yb^{3+}/Ho^{3+}$ UCMPs doped with different Mg^{2+} ion concentrations. With the change in Mg^{2+} ion concentration, the conversion of the ratio of red light to green light of UC luminescence is only about 10%, indicating that the UC luminescence of the sample has good monochromaticity, and is affected only slightly by the concentration of Mg^{2+} ion doping. In Figure 5b, the visible light colors of $LiYF_4:Yb^{3+}/Ho^{3+}$ with different concentrations of Mg^{2+} ion doping are exhibited in the CIE color coordinates (without interference by UV/IR light). The coordinates of $LiYF_4:Yb^{3+}/Ho^{3+}$ UCMPs with different concentrations Mg^{2+} ion doping were (0.2653, 0.5731), (0.2809, 0.5792), (0.2977, 0.5563), (0.2844, 0.6024), (0.2990, 0.6127), and (0.3151, 0.6204), respectively.

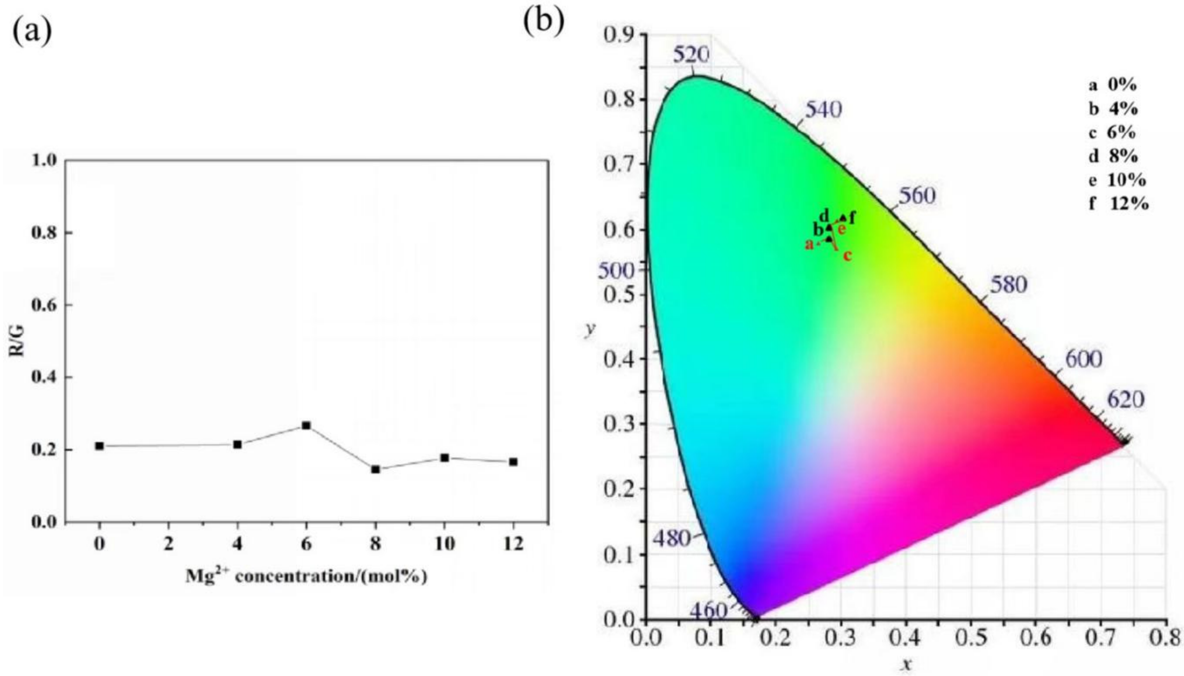

Figure 5. (**a**) Upconversion red–green light intensity ratio of Mg^{2+}-doped $LiYF_4$:Yb^{3+}/Ho^{3+} UCMPs; (**b**) CIE of Mg^{2+}-doped $LiYF_4$:Yb^{3+}/Ho^{3+} UCMPs.

In order to further study the UC luminescence enhancement effect of Mg^{2+} ions on $LiYF_4$:Yb^{3+}/Ho^{3+} UCMPs, the UC luminescence lifetimes at 543 nm and 657 nm of $LiYF_4$:Yb^{3+}/Ho^{3+} UCMPs doped with and without Mg^{2+} ions were measured under 980 nm laser excitation. Then, the corresponding fluorescence lifetimes were calculated by fitting the test results. As shown in Figure 6a,b, the UC fluorescence lifetime of $LiYF_4$:Yb^{3+}/Ho^{3+} UCMPs without Mg^{2+} ion doping at 543 nm was 551.6 μs, and the UC fluorescence lifetime at 657 nm was 361.438 μs. As shown in Figure 6c,d, the UC fluorescence lifetime of 8 mol% Mg^{2+}-ion-doped $LiYF_4$:Yb^{3+}/Ho^{3+} UCMPs at 543 nm was 662.824 μs, and the UC fluorescence lifetime at 657 nm was 639.58 μs. This shows that the UC fluorescence lifetime at 543 nm and 657 nm is increased by about 20% and 70%, respectively, due to doping with Mg^{2+} ions. These results demonstrate that doping with Mg^{2+} ions can significantly enhance the fluorescence lifetime of the samples.

Screen printings were made on various materials, including paper, plastic sheet, and glass sheet. The photographs of the imaging experiments are shown in Figure 7b. All characters' patterns on different materials were almost invisible under daylight conditions. However, the as-printed characters on various materials became green and clearly visible under the excitation of the 980 nm laser. This shows that the $LiYF_4$:Yb^{3+}/Ho^{3+} UCMPs with different Mg^{2+} ion doping have good application potential in anti-counterfeiting recognition.

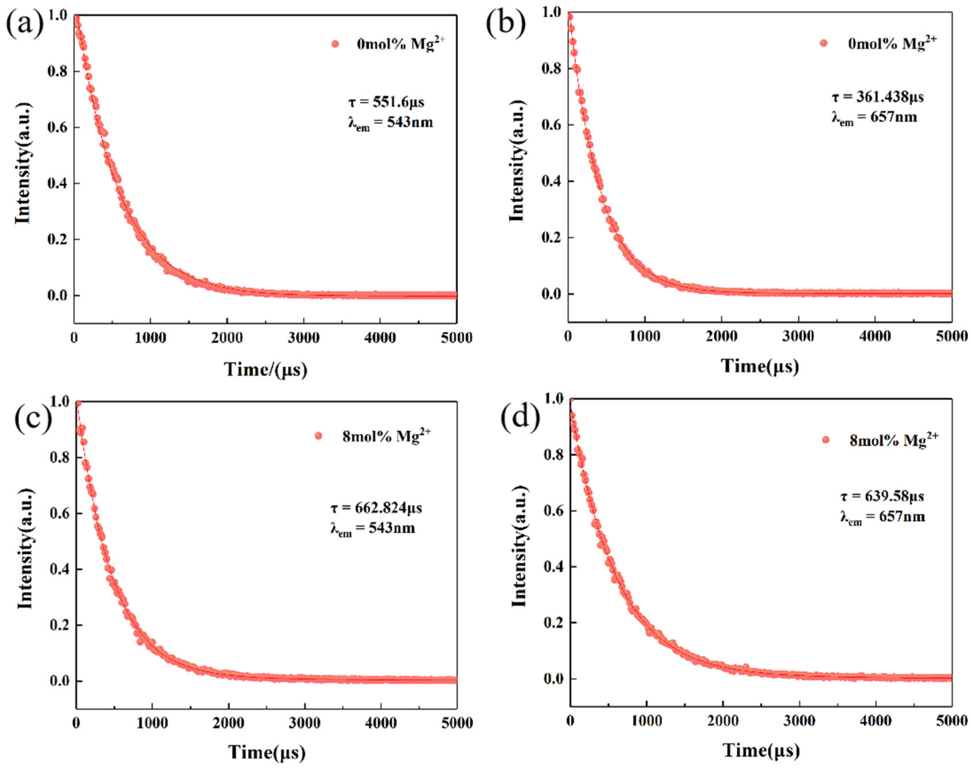

Figure 6. The upconversion fluorescence lifetime decay curves of $LiYF_4$:Yb^{3+}/Ho^{3+} UCMPs doped with (**a**) 0 mol% and (**c**) 8 mol% Mg^{2+} at 543 nm. The upconversion fluorescence lifetime decay curves of $LiYF_4$:Yb^{3+}/Ho^{3+} UCMPs doped with (**b**) 0 mol% and (**d**) 8 mol% Mg^{2+} at 657 nm.

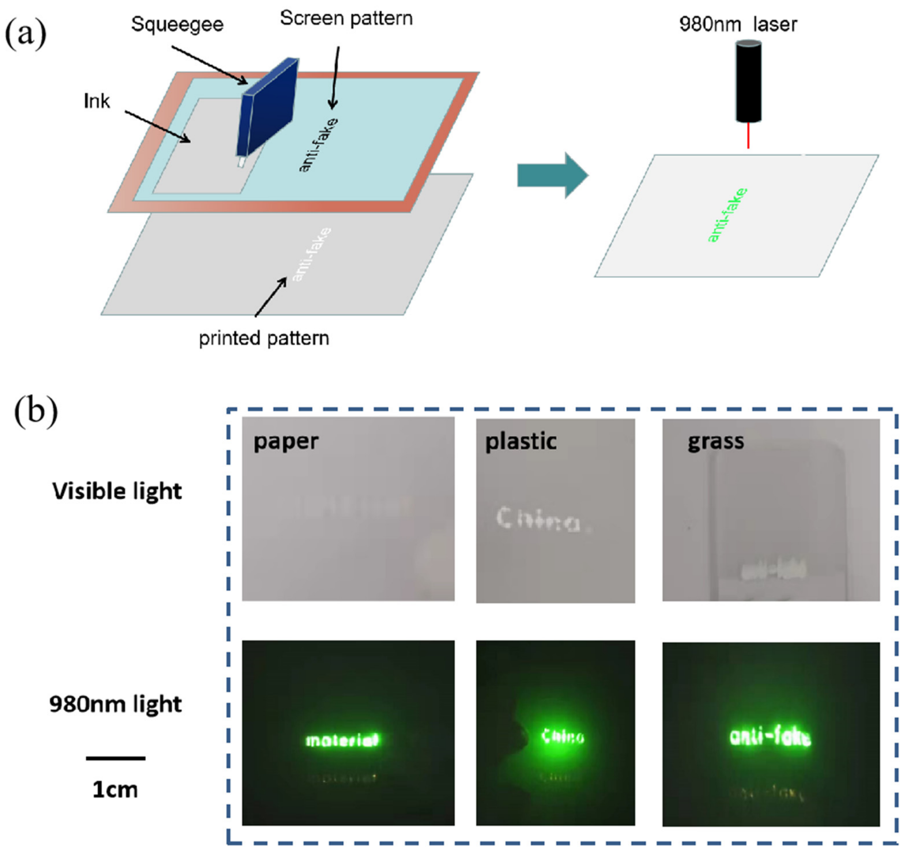

Figure 7. (**a**) Demonstration of the screen-printing process and the anti-counterfeiting application

of 980 nm excitation. (**b**) Photographs of different kinds of anti-counterfeiting characters that were printed onto various materials with the composites as inks under the excitation of a 980 nm laser.

Figure 7a shows the screen-printing process of making anti-counterfeiting characters. Firstly, $LiYF_4:Yb^{3+}/Ho^{3+}$ micron crystal particles doped with a Mg^{2+} ion concentration of 8 mol% were selected as the raw material for anti-counterfeiting ink. The ground $LiYF_4:Yb^{3+}/Ho^{3+}/Mg^{2+}$ micron crystal powder was evenly mixed with mesh metal ink to make anti-counterfeiting ink, which was prepared at a ratio of 5:1 (samples:ink). Finally, the prepared anti-counterfeiting ink was poured onto the screen-printing template, and then brushed with a scraper. The specific anti-counterfeiting characters were successfully printed on the base material below the screen-printing template, and the upconversion luminous anti-counterfeiting characters were obtained.

4. Conclusions

In summary, $LiYF_4:Yb^{3+}/Ho^{3+}$ UCMPs with different Mg^{2+} ion doping concentrations were synthesized and investigated. The emission peaks of Ho^{3+} ions were 480 nm, 535 nm, 543 nm, 638 nm, 657 nm, and 750 nm under the excitation of a 980 nm laser when different concentrations of Mg^{2+} ions were incorporated. The photoluminescence intensity reached its maximum when the Mg^{2+} ion doping concentration was 8 mol%. The prepared UCMPs were incorporated into a screen-printing agent. Characters were printed on different materials using the engraved screen-printing template. The printed characters were clearly visible under the irradiation of a 980 nm laser. The synthesized $LiYF_4:Yb^{3+}/Ho^{3+}/Mg^{2+}$ UCMPs have potential application prospects in anti-counterfeiting recognition.

Supplementary Materials: The following supporting information can be downloaded at: https://www.mdpi.com/article/10.3390/photonics9090614/s1, Table S1: ICP-OES results of LiYF4:$Yb^{3+}/Ho^{3+}/Mg^{2+}$.

Author Contributions: Experimental investigation and analysis, D.L. and J.W.; writing—original draft preparation, D.L.; validation, D.L. and J.W.; writing—review and editing, J.S. and D.L.; supervision, J.S. and C.W. All authors have read and agreed to the published version of the manuscript.

Funding: This research received no external funding.

Institutional Review Board Statement: Not applicable.

Informed Consent Statement: Not applicable.

Data Availability Statement: Not applicable.

Conflicts of Interest: The authors declare no conflict of interest.

References

1. Gai, S.; Li, C.; Yang, P.; Lin, J. Recent progress in rare earth micro/nanocrystals: Soft chemical synthesis, luminescent properties, and biomedical applications. *Chem. Rev.* **2014**, *114*, 2343–2389. [CrossRef] [PubMed]
2. Fan, S.; Gao, G.; Lin, Z.; Li, W.; Fan, S.; Sun, S.; Sun, H.; Hu, L. Highly stable and efficient pure green up-conversion emission of rod-like β-$NaGdF_4:Yb^{3+},Ho^{3+}$ submicro-crystals via ion-exchange for fluorescent labeling. *J. Mater. Chem. C* **2018**, *6*, 5210. [CrossRef]
3. Xu, X.K.; Li, W.; Zhou, W.; Tan, G.P.; Zheng, Y.H.; Hu, C.F.; Lei, B.F.; Zhang, X.J.; Liu, Y.L.; Zhuang, J.L. Preparation and properties of dual-mode luminescent $NaYF_4$:Yb,Tm@SiO_2/carbon dot nanocomposites. *J. Mater. Chem. C* **2018**, *6*, 10360. [CrossRef]
4. Homann, C.; Krukewitt, L.; Frenzel, F.; Grauel, B.; Würth, C.; Resch-Genger, U.; Haase, M. $NaYF_4$:Yb, Er/$NaYF_4$ Core/Shell Nanocrystals with High Upconversion Luminescence Quantum Yield. *Angew. Chem. Int. Edit.* **2018**, *57*, 8765. [CrossRef] [PubMed]
5. Pilch, A.; Wawrzyńczyk, D.; Kurnatowska, M.; Czaban, B.; Samoć, M.; Strek, W.; Bednarkiewicz, A. The concentration dependent up-conversion luminescence of Ho^{3+} and Yb^{3+} co-doped β-$NaYF_4$. *J. Lumin.* **2017**, *182*, 114–122. [CrossRef]
6. Zhou, B.B.; Xu, B.; He, H.M.; Gu, Z.J.; Tang, B.; Ma, Y.; Zhai, T.Y. Enhanced green upconversion luminescence in tetrahedral $LiYF_4$:Yb/Er nanoparticles by manganese(II)-doping: The key role of the host lattice. *Nanoscale* **2018**, *10*, 2834–2840. [CrossRef]
7. Li, Y.B.; Li, X.L.; Xue, Z.L.; Jiang, M.Y.; Zeng, S.J.; Hao, J.H. M^{2+} Doping Induced Simultaneous Phase/Size Control and Remarkable Enhanced Upconversion Luminescence of NaLnF4 Probes for Optical-Guided Tiny Tumor Diagnos. *Adv. Healthc. Mater.* **2017**, *6*, 1601231. [CrossRef]

8. Yang, Y.X.; Xu, Z.; Zhao, S.L.; Liang, Z.Q.; Zhu, W.; Zhang, J.J. Shape controllable synthesis and enhanced upconversion photoluminescence of β-$NaGdF_4$:Yb^{3+}, Er^{3+} nanocrystals by introducing Mg^{2+}. *Chin. Phys. B* **2017**, *26*, 7. [CrossRef]
9. Ding, M.Y.; Ni, Y.R.; Song, Y.; Liu, X.X.; Cui, T.L.; Chen, D.Q.; Ji, Z.G.; Xu, F.; Lu, C.H.; Xu, Z.Z. Li^+ ions doping core–shell nanostructures: An approach to significantly enhance upconversion luminescence of lanthanide-doped nanocrystals. *J. Alloys Compd.* **2015**, *623*, 42–48. [CrossRef]
10. Ding, M.Y.; Cui, S.S.; Fang, L.; Lin, Z.X.; Lu, C.H.; Yang, X.F. NIR-I-Responsive Single-Band upconversion Emission through Energy Migration in Core–Shell–Shell Nanostructures. *Angew. Chem. Int. Ed.* **2022**, *61*, 03631. [CrossRef] [PubMed]
11. Yao, W.J.; Tian, Q.Y.; Liu, J.; Wu, Z.H.; Cui, S.Y.; Ding, J.; Dai, Z.; Wu, W. Large-scale synthesis and screen printing of upconversion hexagonal-phase $NaYF_4$:Yb^{3+},Tm^{3+}/Er^{3+}/Eu^{3+} plates for security applications. *J. Mater. Chem. C* **2016**, *26*, 6327. [CrossRef]
12. Kumar, P.; Singh, S.; Gupta, B.K. Future prospects of luminescent nanomaterials based security ink: From synthesis to anti-counterfeiting applications. *Nanoscale* **2016**, *8*, 1429. [CrossRef] [PubMed]
13. Yao, W.J.; Tian, Q.Y.; Liu, J.; Xue, Q.W.; Li, M.X.; Liu, L.; Lu, Q.; Wu, W. Preparation and RGB Upconversion Optic Properties of Transparent Anti-Counterfeiting Films. *Nanoscale* **2017**, *9*, 15982. [CrossRef] [PubMed]
14. Li, D.D.; Mo, J.Y.; Wang, C.; Wu, Z.W.; Hao, A.H.; She, J.B. Enhanced upconversion emission of $NaGdF_4$: Yb^{3+}/Tm^{3+} crystals by introducing Li^+ ions for anti-counterfeiting recognition. *Appl. Phys. A* **2021**, *127*, 522. [CrossRef]
15. Andres, J.; Hersch, R.D.; Moser, J.E.; Chauvin, A.S. A New Anti-Counterfeiting Feature Relying on Invisible Luminescent Full Color Images Printed with Lanthanide-Based Inks. *Adv. Funct. Mater.* **2014**, *24*, 5029. [CrossRef]
16. Yi, J.; Qu, J.B.; Wang, Y.A.; Zhou, D.C. Preparation and characterization of nanosized $GdxBi_{0.95-x}VO_4$: 0.05Eu^{3+} solid solution as red phosphor. *Chin. Phys. B* **2014**, *23*, 104224. [CrossRef]
17. Yang, J.Z.; Qiu, J.B.; Yang, Z.W.; Song, Z.G.; Yang, Y.; Zhou, D.C. Preparation and upconversion luminescence properties of $Ba_5SiO_4Cl_6$: Yb^{3+}, Er^{3+}, Li^+ phosphors. *Acta Phys. Sin.* **2015**, *64*, 138101. [CrossRef]
18. Li, W.C.; Xu, J.X.; He, Q.; Sun, Y.; Sun, S.Y.; Chen, W.; Guzik, M.; Boulon, G.; Hu, L.L. Highly stable green and red up-conversion of $LiYF_4$:Yb^{3+}, Ho^{3+} for potential application in fluorescent labeling. *J. Alloys Compd.* **2020**, *845*, 155820. [CrossRef]